THE ASTROPHYSICAL JOURNAL, 266:309–320, 1983 March 1

DENSE CORES IN DARK CLOUDS. II. NH_3 OBSERVATIONS AND STAR FORMATION

P. C. MYERS[1,2] AND P. J. BENSON[1,3]
Received 1982 June 7; accepted 1982 August 18

ABSTRACT

We present partial results of a survey of ~100 visually opaque regions in nearby dark clouds in the 1.3 cm $(J, K) = (1, 1)$ line of NH_3, with mapping of all strong sources ("dense cores") and (2, 2) line observations in selected positions. For 27 dense cores with distance estimates, mean properties are: FWHM diameter, 0.1 pc; density, 3×10^4 cm^{-3}; mass, 4 $M_\odot$; kinetic temperature, 11 K; and FWHM velocity width, 0.3 km s^{-1}. We compare line shapes with cloud motion models, and source density, size, and temperature with equilibrium and stability requirements. These indicate that most dense cores are in the early stages of collapse or in near-critical equilibrium; if in equilibrium, they are probably supported by a combination of thermal and subsonic turbulent motions. In Taurus-Auriga, positions of the 10 known dense cores are well correlated with positions of emission-line star groups. In the next dense core free-fall time, 2×10^5 yr, the Taurus-Auriga complex is expected to form 25–50 emission-line stars. This is consistent with the estimated number of dense cores, 25. Taken together, these results suggest that most of the dense cores described here will form low-mass stars in the next ~10^6 yr.

Subject headings: interstellar molecules — nebulae: general — stars: formation

I. INTRODUCTION

Young stars are often found near visible obscuration (Joy 1945, 1949; Ambartsumian 1947; Herbig 1962) and/or near regions of strong molecular line absorption (Zuckerman *et al.* 1970) or emission (Wilson *et al.* 1974). It is often suggested that molecular clouds, or parts of molecular clouds, are collapsing to form such young stars because their thermal pressure is too small to support them against collapse (Goldreich and Kwan 1974). However, these general connections between gas clouds and young stars are not detailed enough to predict where or when the next stars will form in a molecular cloud, for several reasons: (1) not all molecular clouds have evidence of the presence of young stars; (2) many cloud regions which appear unstable if supported thermally appear stable if supported by the "turbulent pressure" corresponding to their line widths (Larson 1979, 1981); (3) the rate of star formation in the Galaxy is consistent with only a small fraction of the known cloud mass converting to stars on free-fall time scales (Zuckerman and Palmer 1974). Therefore, it is uncertain which condensations in a molecular cloud will form stars, and when. By itself, the presence of condensations in optical photographs or molecular line maps does not necessarily imply that stars are forming, or will form, in them.

In this paper we present observation and analysis of emission from nearby dark clouds in Taurus and elsewhere, in the $(J, K) = (1, 1)$ and (2, 2) lines of NH_3 at 1.3 cm wavelength. In combination with stellar data, these results suggest that it is possible to specify, with more certainty than before, which condensations are likely to form stars in the next ~10^6 years. Many of these condensations appear destined to form low-mass stars because, (1) if they are not now collapsing, their stability appears close to critical; (2) their spatial distribution appears correlated with groups of emission-line stars; and (3) the number of such regions is consistent with the number of stars expected to form in the next free-fall time.

The results are based on an extensive program of observations of dense cloud cores. The selection of the regions to be studied, and CO observations of them, were presented in Myers, Linke, and Benson (1983, hereafter Paper I); a more detailed description of the NH_3 observations will be given later. In this paper the observations are described briefly in § II; the results are analyzed in terms of possible cloud motions in § III; the relation of the NH_3 emission regions to young stars is described in § IV; the results are discussed in § V, and the paper is summarized in § VI.

II. OBSERVATIONS

The observations of the NH_3 $(J, K) = (1, 1)$ and (2, 2) lines at 1.3 cm wavelength were made during the winters of 1980 and 1981 at the 43 m telescope of the National Radio Astronomy Observatory (NRAO)[4] and during several sessions in 1980, 1981, and 1982 with the

[1] Department of Physics and Research Laboratory of Electronics, Massachusetts Institute of Technology.
[2] Visiting Scientist, Harvard-Smithsonian Center for Astrophysics.
[3] Amelia Earhart Fellow.

[4] The National Radio Astronomy Observatory is operated by Associated Universities, Inc., under contract with the National Science Foundation.

37 m telescope of Haystack Observatory.[5] The NRAO observations had a 1.2 beamwidth and a 0.25 beam efficiency, and used a maser receiver with a system temperature of 50–70 K. The spectra were taken using frequency switching. The spectrometer was a digital autocorrelator with 384 channels (1980) or 1024 channels (1981). The analyzed bandwidth was 5.0 MHz, giving a velocity resolution of 0.20 km s^{-1} (1980) or 0.075 km s^{-1} (1981). The Haystack observations were made with 1.4 angular resolution, and with sensitivity and spectral resolution similar to those of the 1981 NRAO observations. All spectra were corrected for atmospheric attenuation and for variation of gain with elevation (Haystack) or hour angle (NRAO). The Haystack observations were used for surveying and mapping in the (1, 1) line; the NRAO observations were made in the (1, 1) and (2, 2) lines at selected cloud positions primarily to estimate gas temperatures.

[5] Radio astronomy at the Haystack Observatory of the Northeast Radio Observatory Corporation is supported by the National Science Foundation.

Approximately 100 positions of high visual extinction were surveyed for NH_3 (1, 1) line emission; most of these coincide with positions in Table 3 and Table 4 in Paper I. The search procedure involved a single 30 minute spectrum on each position, followed by partial or full mapping around the stronger detections. In a few cases, we mapped around positions of weak or negative detections, guided by the presence of strong $C^{18}O$ emission (Paper I). The typical rms variation in antenna temperature in one channel was 0.08 K. This search resulted in 39 clouds where the main hyperfine feature had an antenna temperature $T_A \gtrsim 0.4$ K in at least one position, and 31 clouds where the satellite hyperfine features were strong enough compared with the noise to analyze with the 18 component Gaussian fitting program described in Benson and Myers (1980, hereafter BM). Thirty-two clouds were mapped with 1′ spacing, to define the contour of half-maximum intensity in the main hyperfine feature. Of these clouds, 27 have reliable distance estimates. Table 1 presents observed and derived parameters for these 27 clouds and the mean and standard deviation in these quantities. Each given

TABLE 1

OBSERVED AND DERIVED SOURCE PROPERTIES

Source	α(1950)	δ(1950)	V_{LSR} (km s^{-1})	ΔV (km s^{-1})	$\Delta\theta_x \times \Delta\theta_y$ (arcmin)	D (pc)	R (pc)	T_k (K)	log n	M ($M_\odot$)	Ref.
L1489	04^{h}01^{m}45.0	26°11′33″	6.65	0.28	2.0 × 1.4	140	0.068	10	4.3	0.57	1
L1498	04 07 50.0	25 02 13	7.71	0.20	1.8 × 1.3	140	0.063	10	4.2	0.36	1
L1495	04 11 06.5	28 01 53	6.77	0.24	2.0 × 1.9	140	0.079	(10)	4.4	1.1	1
L1400G	04 21 05.1	54 52 20	3.42	0.30	3.3 × 1.6	170	0.11	10	3.9	0.96	2
B217	04 24 42.5	26 11 13	6.91	0.33	2.3 × 1.1	140	0.065	(11)	5.1	3.1	1
L1400K	04 06 51.0	54 45 27	3.24	0.32	3.6 × 1.5	170	0.12	(10)	3.7	0.78	2
L1551	04 28 35.8	18 02 52	6.49	0.51	3.5 × 1.5	140	0.093	11	4.8	4.6	1
TMC-2A	04 28 54.0	24 26 27	5.85	0.32	2.1 × 1.8	140	0.079	(10)	4.7	2.2	1
TMC-2	04 29 43.0	24 18 54	6.19	0.27	3.9 × 2.9	140	0.14	10	4.4	6.2	1
L1536	04 30 26.0	22 37 10	5.57	0.22	4.1 × 2.0	140	0.12	10	4.5	5.0	1
TMC-1C	04 38 34.5	25 55 00	5.18	0.26	6.2 × 2.3	140	0.15	10	4.1	3.9	1
TMC-1	04 38 19.0	25 42 30	5.88	0.38	16 × 2	140	0.23	(10)	4.1	14	1
L1517B	04 52 07.2	30 33 18	5.67	0.20	2.3 × 2.1	140	0.090	10	3.8	0.42	1
L1512	05 00 54.4	32 39 00	7.05	0.21	1.8 × 0.8	140	0.049	(10)	5.1	1.3	1
L1544	05 01 14.0	25 07 00	7.14	0.32	2.8 × 2.3	140	0.10	10	4.0	0.91	1
L134A	15 50 58.1	−04 26 36	2.67	0.34	3.5 × 2.2	100	0.081	10	4.5	1.5	3
L183	15 51 35.7	−02 40 54	2.41	0.24	8 × 2	100	0.12	10	4.3	3.1	3
L1696A	16 25 30.0	−24 11 32	3.37	0.29	3.6 × 0.8	160	0.079	(15)	4.3	0.89	4
L43	16 31 42.0	−15 41 00	0.67	0.40	3.6 × 1.9	160	0.12	12	4.1	2.0	4
L234A	16 45 21.0	−10 46 33	2.86	0.23	2.8 × 2.1	160	0.11	10	4.2	1.9	4
L234E	16 45 18.5	−10 51 43	3.03	0.30	1.9 × 1.6	160	0.081	15	3.7	0.24	4
L63	16 47 21.0	−18 01 00	5.73	0.26	2.9 × 2.3	160	0.12	(10)	4.5	5.0	4
B335	19 34 33.3	07 27 00	8.32	0.40	1.8 × 1.3	400	0.18	(10)	3.7	2.7	5
L1152	20 35 17.4	67 43 16	2.46	0.42	2.8 × 1.6	440	0.27	10	3.9	14	6
L1174	20 59 46.3	68 01 04	2.83	0.74	2.7 × 1.6	440	0.27	(15)	4.2	28	6
L1172	21 01 48.6	67 42 13	2.74	0.36	1.5 × 1.1	440	0.16	11	4.0	3.7	6
L1262	23 23 32.2	74 01 45	3.86	0.37	2.9 × 1.2	200	0.11	10	3.9	0.96	7
Mean	...	...	...	0.32	3.6 × 1.7	...	0.12	10.5	4.4	4.1	
S.D.	...	...	...	0.11	2.8 × 0.5	...	0.06	1.2	4.5	5.8	
Points	...	...	...	27	27	...	27	17	27	27	

NOTE.—Estimated distance D is based on the reference given in the twelfth column. When the kinetic temperature, T_k, was not deduced because (2, 2) line observations were not made, the assumed value is given in parentheses. The means and standard deviations are calculated for the quantities in the corresponding column, except for log n. There, the "mean" is the log of the mean density and the "S.D." is the log of the standard deviation. The sizes for TMC-1 and L183 are taken respectively, from Little *et al.* 1979 and Ungerechts, Walmsley, and Winnewisser 1980. All maps were made with 1.0 spacing, except for L1551, which was mapped with 1.5 spacing (Buxton 1981).

REFERENCES.—(1) Elias 1978*a*; (2) Snell 1981, assuming D(L1400) = D(L1407); (3) Mattila 1979; (4) Elias 1978*b*; (5) Bok and McCarthy 1974; (6) Elmegreen and Elmegreen 1978; (7) Snell 1981, assuming D(L1262) = D(L1257).

position is the position of peak emission intensity. The quantities V_{LSR} and ΔV are, respectively, the center velocity with respect to the local standard of rest and intrinsic FWHM line width, as described by BM. Each cloud map was fitted with a two-dimensional Gaussian function. The FWHM angular sizes, $\Delta\theta_x$ and $\Delta\theta_y$ represent intrinsic source size along the major and minor axes, after deconvolution of the best fit map with the telescope beam. The corresponding beam filling factor was typically 0.8. The adopted source distances, D, are based on the optical estimates cited in column (12). The linear size is $R = D(\Delta\theta_x \Delta\theta_y)^{1/2}$, the geometric mean FWHM diameter. In Paper I, it is shown that the column density through a centrally condensed, isothermal, pressure-bounded equilibrium sphere has a FWHM approximately equal to the sphere radius. In the comparison made in § III, we take R to be this radius.

The number density of H_2 and He, $n = 1.2n(H_2)$, and the kinetic temperature, T_k, were determined from statistical equilibrium excitation models of the (1, 1) and (2, 2) lines, as described in detail by BM. Briefly, the (1, 1) spectra were fitted by assuming that the optical depth at each frequency is the sum of 18 Gaussian components, with local thermodynamic equilibrium (LTE) relative values, and with relative separations corresponding to the magnetic hyperfine structure of the transition (Kukolich 1967). Each component was assumed to have the same excitation temperature, T_{11}, and the same FWHM, Δv. The four fitted parameters are then the LSR velocity, τ_0 (the sum of all 18 peak optical depths), T_{11}, and Δv. At the peak of the main hyperfine feature, the optical depth is typically 2–3. At the peaks of the satellite features, the optical depth is typically less than 0.5. Then T_{11} and τ_0 were used in solving a system of four equations in the four unknowns: N_{22} [column density in the upper (2, 2) inversion level], T_{22} [excitation temperature of the (2, 2) transition], n, and T_k. The equations are (1) an expression for T_{11} (n, T_k) based on a two-level excitation model, including effects of background radiation and trapping (Martin and Barrett 1978; Scoville and Solomon 1974); (2) a similar expression for T_{22} (n, T_k); (3) the solution to the plane-parallel equation of radiative transfer for the optically thin (2, 2) line in a uniform medium, giving N_{22} (T_{22}); and (4) the Boltzmann relation for N_{22} (N_{11}, T_{21}), where N_{11} is known from the best fit values of (1, 1) line opacity and T_{11}. The rotation temperature T_{21} relates the upper-state populations of the (2, 2) and (1, 1) doublets and is essentially equal to T_k. These excitation models use the rate constants, R, of Green (1980) and allow for NH_3 collisions with He and H_2 molecules, according to $R(NH_3 - H_2)/R(NH_3 - He) = 1.7$. This factor is due primarily to the He/H_2 mass ratio. The values of n and T_k derived from these calculations are generally in good agreement with densities derived from H_2CO observations and temperatures based on ^{12}CO observations (Snell 1981). When (2, 2) line observations were not made, it is usually assumed that $T_k = 10$ K, in accord with ^{12}CO observations. The mass, M, of each source is the mass of a sphere of diameter R and uniform density n. Therefore, M is approximately the mass enclosed by the half-maximum map contour.

The typical dense core is seen to have a 0.32 km s^{-1} line width, 0.1 pc size, 11 K kinetic temperature, a density of 3×10^4 cm^{-3}, and a 4 $M_\odot$ mass. The uncertainty in width is typically 0.02 km s^{-1} and, in kinetic temperature, is 1 K. The estimated relative uncertainties in size, density, and mass are, respectively, a factor of 1.5, 2.5, and 5.

III. CLOUD MOTIONS

We have analyzed the line shapes and possible equilibrium of the observed clouds in order to assess their internal motions. The line shape analysis was done on six spectra with extremely narrow intrinsic line widths ($\Delta v \leq 0.25$ km s^{-1}) and sufficiently high signal-to-noise. We estimated the intrinsic line shape by taking spectral features having relatively little contamination and averaging them to reduce noise fluctuations. This procedure is illustrated in Figures 1*a* and 1*b*. Figure 1*a* shows the observed NH_3 (1, 1) spectrum of L1498, with some baseline channels between spectral features cut away to reveal the features more clearly. Below the observed spectrum is the best fit model spectrum (BM), with vertical strokes indicating the expected component spacing and optically thin, LTE relative intensities (Kukolich 1967). Among the spectral features labeled 1–8, features 2, 3, 5, 6, 7, and 8 are relatively uncontaminated by emission from more than one component. Figure 1*b* shows the average of these features as filled circles, on a velocity scale expanded by a factor of ~ 20.[6]

The spectrum in Figure 1*b* is representative of the six which were analyzed, in its agreement or disagreement with the models of cloud motion which we considered. The spectra expected from these models are shown in Figure 1*b* as solid lines. The curve labeled "static 10 K" is the expected optically thin NH_3 spectrum from a uniform 10 K cloud with only thermal motions. Since the peak optical depth of the hyperfine satellites is typically less than 0.5, optical depth broadening of the line is expected to be negligible. The calculation was done for a 10 K cloud because the NH_3 observations of this source indicate $T_k = 10$ K (Table 1). However the curve is clearly narrower than the observed spectrum. The curve labeled "collapse 10 K" was obtained by using the 1 $M_\odot$ collapse model in Figure 10 of Larson (1972) to predict the spectrum of optically thin NH_3 emission, assuming (1) there is negligible variation in NH_3 abundance and excitation temperature across the cloud; (2) the cloud is 140 pc distant (Elias 1978*a*); and (3) it is observed with a circularly symmetric Gaussian beam of 1.'4 FWHM. This model represents a well-developed collapse, approximately two free-fall times (4×10^5 yr) old, when half of the total mass has accreted onto a stellar core. The model curve exhibits

[6] It may be possible to extract the intrinsic line shape from blended components more rigorously by use of Fourier transform techniques (Ball 1975).

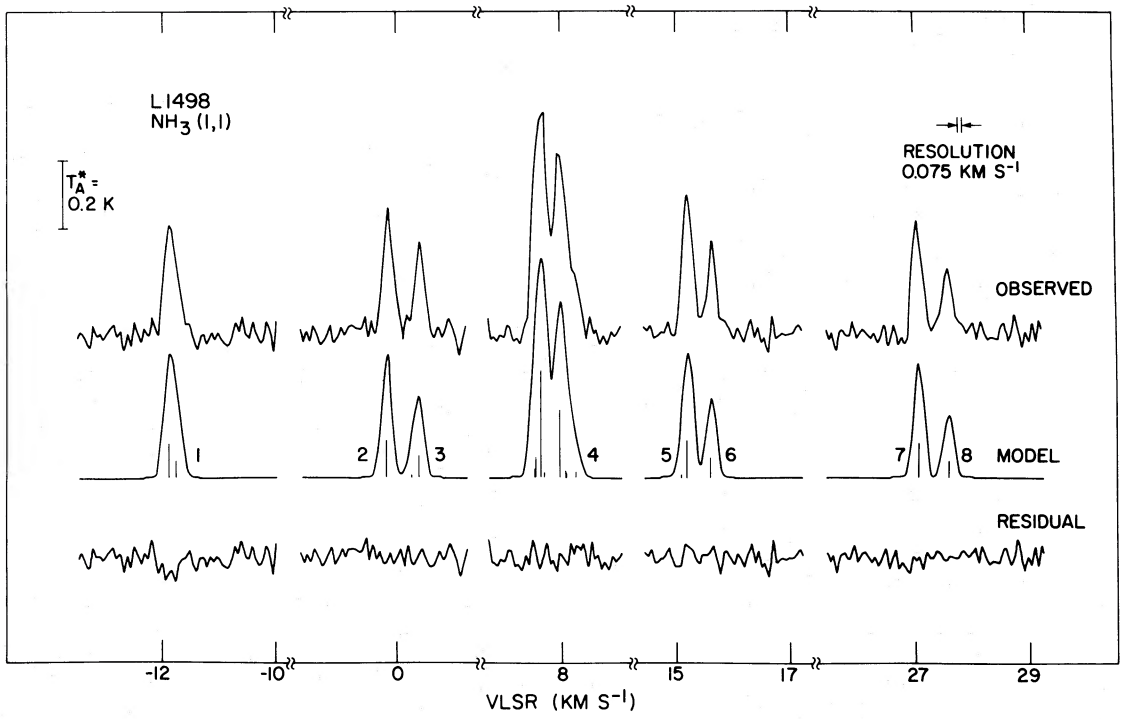

FIG. 1*a*

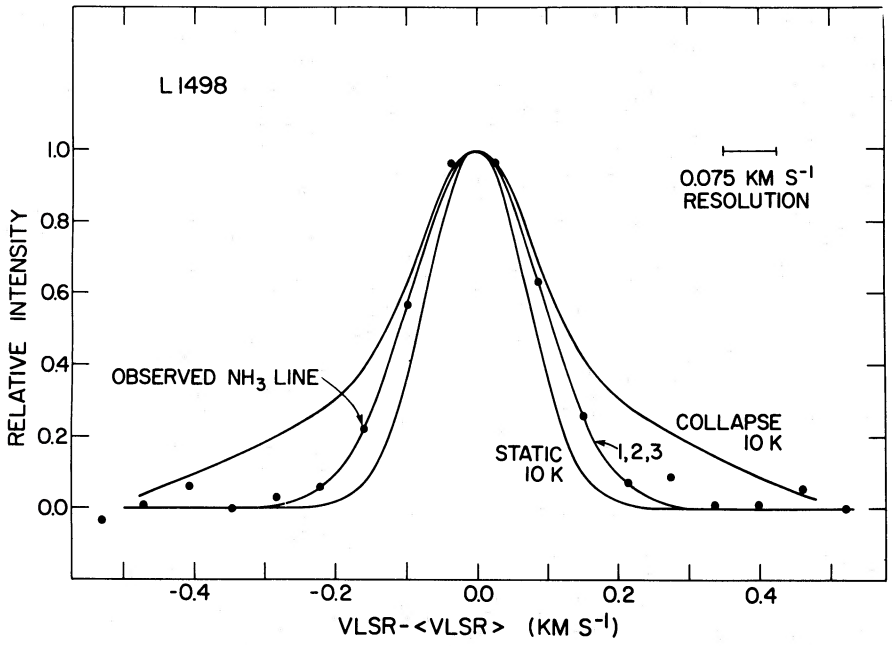

FIG. 1*b*

FIG. 1.—(*a*) Observed and best fit model spectra of NH_3 (1, 1) emission from L1498, with interfeature channels cut away to reveal spectral details. Vertical strokes indicate relative spacing of the 18 hyperfine components and their optically thin LTE relative intensities. Lower spectrum shows residual after best fit model spectrum is subtracted from observed spectrum. (*b*) Comparison of intrinsic NH_3 (1, 1) line shape in L1498 (*filled circles*) with model predictions (*solid lines*). The intrinsic line shape was estimated by averaging the features labeled 2, 3, 5, 6, 7, and 8 in Fig. 1*a*. See text for model details. The comparison indicates that the line shape is best fitted by a 10 K cloud with either subsonic microturbulence or early ($< 1 \times 10^5$ yr) collapse.

wings which are absent in the observed spectrum. If the observed cloud is collapsing in the manner of this model, it must be at a significantly earlier stage than 4×10^5 yr, such that the wing intensity is reduced by a factor $\gtrsim 3$. The collapse calculations of Shu (1977) indicate that the fraction of all cloud gas having collapse speed greater than 0.2 km s^{-1} increases by a factor of ~ 3 as the time from the start of the collapse increases by a factor of ~ 6, within the time interval from 3×10^4 yr to 2×10^5 yr. Although these two calculations differ in several details, this comparison suggests that consistency between the observed spectrum and Larson's collapse model probably requires that the collapse be younger than 1×10^5 yr, i.e., prior to the formation of a stellar core. We note that this comparison applies to narrow lines and small (1 $M_\odot$) clouds. Collapse models of larger clouds (e.g., the 10 $M_\odot$ model of Larson 1972) predict broader lines and enhanced wings compared with those in Figure 1*b*. However, none of the NH_3 lines in our survey have obvious wings.

The curves labeled "1, 2, 3" represent three physically different models which give the same line shape, which is a Gaussian and which fits the observed data well. Model 1 is for a cloud with purely thermal motions, with a kinetic temperature of 16 K; however, this temperature conflicts with the value of 10 K $\pm$ 1 K deduced from the excitation analysis. It appears that even the narrowest of the observed NH_3 lines is slightly broader than the thermal width.

Model 2 is for a uniform, 10 K cloud with enough rigid-body rotation to broaden the line to the width of the observed spectrum in Figure 1*b*. The cloud is assumed to have a radius of 0.06 pc at a distance of 140 pc; it is rotating about an axis inclined at angle i with respect to the line of sight; and it is observed with the same telescope beam as in the collapse model. The necessary angular speed is then $\omega \sin i = 2.5$ km s^{-1} pc^{-1}. This amount of rotation is small in its contribution to the line width but implies a significant shift in the velocity of peak line emission as one scans across the cloud—a shift which is not usually evident in our data. The expected shift is illustrated in Figure 2 for three beam positions along a line perpendicular to the direction of the rotation axis. The magnitude of the shift from position 1 to position 3 is 0.16 km s^{-1} or approximately one FWHM line width. For clouds with broader lines, the necessary shift increases.

We have sufficient spectra and sensitivity in ~ 10 of our cloud maps to recognize such a gradient in the velocity of peak emission, but it appears in three or more adjacent positions in only a few of these maps. The most detailed examination can be made in the two largest sources, L63 and TMC-1C, with the most extensive mapping data (~ 15 velocity measurements in each source). In L63 a gradient is present, but the total velocity shift is ~ 0.10 km s^{-1} while the intrinsic width is ~ 0.25 km s^{-1}. In TMC-1C there are two localized velocity gradients. The largest shift is ~ 0.20 km s^{-1}, while the intrinsic width is again ~ 0.25 km s^{-1}. Generally, the rms in the velocity of peak line emission for the 5–15

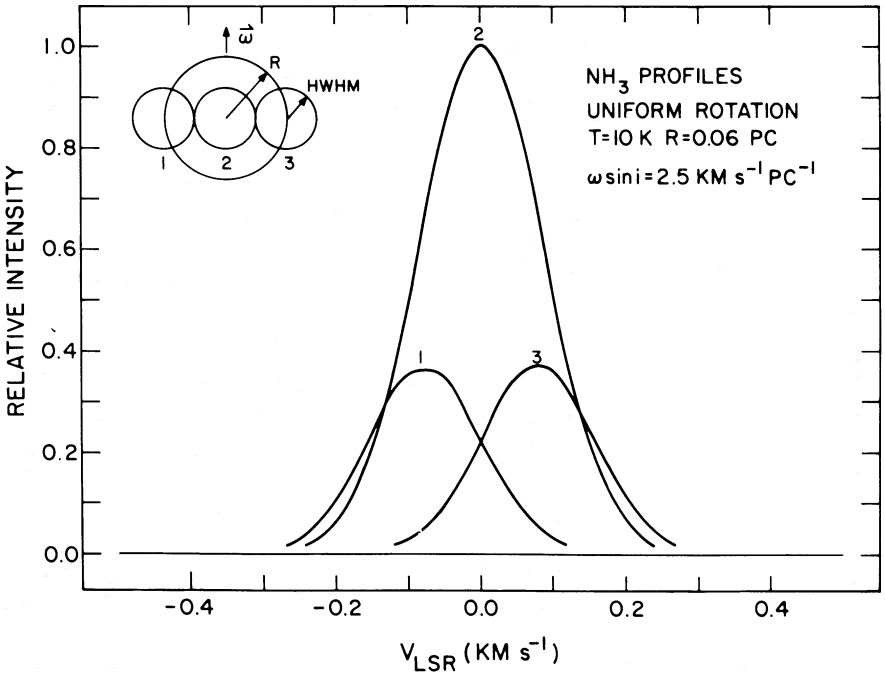

FIG. 2.—Predicted NH_3 (1, 1) line shapes for a uniform 10 K model cloud with enough rigid body rotation to reproduce the observed line shape in Fig. 1*b*. The telescope beam is assumed to step along a line perpendicular to the projected rotation axis, as shown by positions 1, 2, and 3 in the upper left drawing. The predicted spectra, also labeled 1, 2, and 3, show a shift in velocity of peak emission of 0.16 km s^{-1} or approximately one FWHM. No such shift is seen in most of the clouds described here.

spectra in a map is smaller than the intrinsic line width. These results are similar to those of Ungerechts, Walmsley, and Winnewisser (1982), who found detectable velocity gradients in four of eight dense cores, with NH_3 observations of finer angular resolution. However, in only one case (L1535) does the shift in the velocity of peak emission exceed the intrinsic line width. We conclude that simple rotational motion is not generally the dominant source of superthermal line broadening, although it may be important in a few clouds. More complex rotational motion, in which the inner regions rotate faster than the outer regions, could conceivably produce significant broadening but less shift. However, we see little evidence for enhanced broadening in the interiors of our maps.

Model 3 is for a 10 K cloud with sufficient microturbulence to broaden the line to the width observed in Figure 1*b*. The FWHM of the necessary turbulent motion is 0.14 km s^{-1}. This may be compared with the sound speed of the gas at 10 K, assuming that there is one He atom for every five H_2 molecules. The sound speed is then 0.19 km s^{-1} (isothermal) or 0.24 km s^{-1} (adiabatic). The turbulent motions needed to account for the line width are obviously subsonic in this case. In the more typical case, where the observed line width is 0.32 km s^{-1}, the FWHM of the necessary turbulent motions is 0.27 km s^{-1}. For an isotropic Gaussian distribution of turbulent velocities, this corresponds to subsonic speeds for 0.6 (isothermal) or 0.8 (adiabatic) of the turbulent elements. Thus for most of the regions in Table 1, turbulent line broadening, if present, is primarily subsonic. Such turbulence does not face the well-known objection against supersonic turbulence concerning its short dissipation time (Goldreich and Kwan 1974; Field 1978). Furthermore, there appears to be no conflict between this interpretation of the line broadening and other observations.

Of the five cloud motion models thus considered, one—10 K thermal motions plus subsonic microturbulence—appears to have no conflict with the observations. Another—early collapse with an age of less than 1×10^5 yr—may also be consistent, but the consistency is less clear because of the idealized nature of the model and the uncertainties involved in applying it to the data.

The second approach we have used to study possible cloud motions involves comparison of the size, density, and temperature of the observed clouds with conditions for equilibrium and stability of a pressure-bounded isothermal sphere (Ebert 1955; Bonnor 1956; Spitzer 1968, 1978; Paper I). Although this model is also idealized, its use here is probably more realistic than the well-known Jeans length analysis. Of the 27 clouds to which this model is applied, only four have elongation significantly greater than a factor of ~ 2. Therefore, departure from spherical shape probably does not affect the results significantly. To summarize, equilibrium is possible if the external pressure, p_{ext}, at the sphere radius, R, satisfies

$$p_{ext} \leq p_{ext,max} \equiv \frac{3}{4\pi G}\left(\frac{kT}{mR}\right)^2 , \quad (1)$$

where m is the mean mass per particle and T is the temperature characteristic of the supporting motions. If equilibrium is not possible, the cloud should collapse. If equilibrium is present, it is stable if the mean density, n, satisfies

$$n \leq n_{max} \equiv 2.44 \frac{p_{ext,max}}{kT} = 8.44 \frac{T}{R^2} \text{ cm}^{-3} , \quad (2)$$

where R is in pc. If equation (2) is solved for R in terms of n_{max} and T, it is very similar to the expression for the Jeans length. In practice one can make only a crude test for the possibility of equilibrium because of the obvious difficulty in specifying the pressure over a thin surface region from observations. However, it is plausible that the temperature just outside the spherical region of interest is equal to that inside. Then equations (1), (2), and the ideal gas law imply that equilibrium is possible if the external density, n_{ext}, at R satisfies

$$n_{ext} \leq 0.41 n_{max} . \quad (3)$$

The conditions in equations (2) and (3) are similar and are interdependent if n_{ext} and n are related. It appears reasonable to assume that n_{ext} lies in the range

$$0.1n \leq n_{ext} \leq n . \quad (4)$$

The lower limit on n_{ext}, $0.1n$, comes from estimates of the mean density, typically 3×10^3 cm^{-3}, based on ^{13}CO observations of clouds similar to those observed here but over more extended regions (~ 0.5 pc; Langer *et al.* 1980; Snell 1981). The upper limit on n_{ext}, n, comes from the expectation that the core regions under consideration are density maxima.

With these assumptions, the equilibrium conditions can be crudely examined in terms of n, the mean density in the sphere, which is estimated from the observations. Accordingly, the values of n/n_{max} can be divided into three groups: (*a*) $n/n_{max} > 4.1$: equilibrium is impossible and the cloud should be collapsing; (*b*) $0.41 \leq n/n_{max} \leq 4.1$: equilibrium may or may not be possible; if equilibrium is present, it is (i) *unstable* for $1 < n/n_{max} < 4.1$, (ii) *critical* for $n/n_{max} = 1$, (iii) *stable* for $0.41 \leq n/n_{max} < 1$; and (*c*) $n/n_{max} < 0.41$: equilibrium is possible; if present, it is stable.

These conditions are compared with the values of n, T, and R deduced from the observations in Table 1 in Figure 3, which is a plot of log (n/T) versus log R for (*a*) purely thermal supporting motions ($T = T_k$) and (*b*) Doppler supporting motions $[T = 369\ (\Delta v)^2]$. The curves corresponding to $n/n_{max} = 4.1$, $n/n_{max} = 1$, and $n/n_{max} = 0.41$ are also shown; they are straight lines of slope -2, as is evident from equation (2).

Figure 3*a* shows that, if these clouds are supported only by thermal motions, they are generally not in equilibrium and should be collapsing, or their equilibrium is unstable. Figure 3*b* shows that, if they are supported by the Doppler motions in their linewidths, they are again either not in equilibrium, or their equilibrium is close to being critically stable. In this case, the data points lie remarkably close to the critical line. The best fit line through the data points is log $(n/T_D) =$

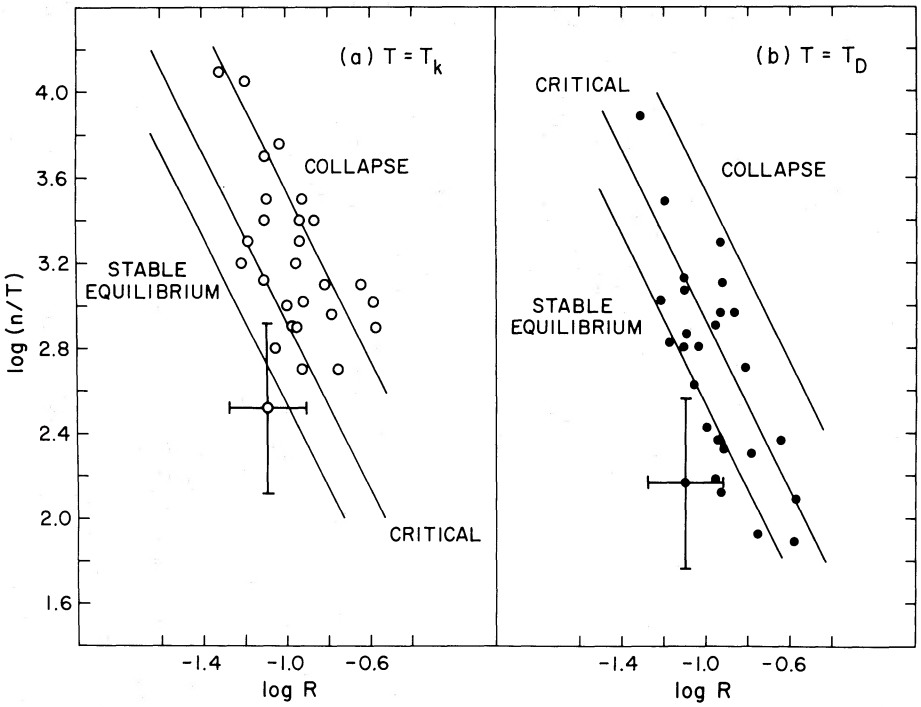

FIG. 3.—Comparison of cloud density, n, in cm^{-3}, temperature, T, in K, and size, R, in pc with requirements for equilibrium and stability, for the two extreme assumptions that supporting motions are due: (*a*) only to the thermal part of line broadening ($T = T_k$); and (*b*) to entire line broadening ($T = T_D$). The solid lines of slope -2 are based on a model of an isothermal, pressure-bounded equilibrium sphere, as described in the text. Points above the upper line represent clouds with no possible equilibrium; they should be collapsing. Points between the upper and lower lines may or may not have possible equilibrium; this cannot be determined from the present data. If a cloud in this region is in equilibrium, the equilibrium is unstable if the point is above the middle (critical) line and stable if the point is below the critical line. Points below the lower line represent clouds in stable equilibrium. Errors bars reflect estimated uncertainties of a factor of 2.5 in n and 1.5 in R. The figure shows that if clouds have only thermal support, most of them are collapsing or unstable. If clouds have Doppler support, they are collapsing or near to critical equilibrium.

$0.95 - 1.8 \log R$, with correlation coefficient $r = 0.69$, while the critical line has $\log (n/T_D) = 0.93 - 2.0 \log R$. The standard deviation of the data points about the critical line is only slightly greater than the standard deviation of the data points about their best-fit line. The correlation of $\log (n/T_D)$ with $\log R$ is slightly more significant than either the correlation of $\log n$ with $\log R$ ($\log n = 3.3 - 1.0 \log R$, $r = 0.49$) or the correlation of $\log T_D$ with $\log R$ ($\log T_D = 2.3 + 0.80 \log R$, $r = 0.57$), so it appears that the correlation corresponding to critical stability is the best defined one among the three variables. This behavior can be understood in terms of the discussion by Shu (1977) of isothermal spheres in equilibrium or in early collapse after a small perturbation from equilibrium. As long as the outer parts of the cloud can communicate acoustically, they will tend to remain in detailed mechanical balance, even if the inner part is collapsing. Therefore, they will appear to be in critical equilibrium when viewed with resolution comparable to the size of the cloud.

Although the line shape and equilibrium analyses in this section present several alternatives, they have a common interpretation: most of the observed clouds are consistent with the early stages of collapse or with near-critical equilibrium involving subsonic turbulent support. For giant molecular clouds, or for larger regions of the clouds considered here, the interpretations of collapse and equilibrium appear distinct, and efforts to choose between them are well known (Goldreich and Kwan 1974; Zuckerman and Evans 1974). However, for the small narrow-line regions, these possibilities seem closer together. If they are collapsing, it is early collapse; if they are in equilibrium, it is near-critical equilibrium. Therefore, it may be worth considering whether these two interpretations are always distinguishable in practice, or even in principle. The discussion by Shu (1977), summarized above, applies to an idealized cloud where turbulent motions are absent. When they are present, the picture is likely to be more complicated. However, it has been suggested that, when turbulent gravitational collapse occurs, the two kinds of motion may act so that virial balance is closely satisfied during the collapse (Larson 1981).

Therefore, the present data and analysis give two choices of equilibrium and collapse, as for larger clouds; each of the two choices appears closer to the onset of collapse than for larger clouds; and it is possible that the two choices are not always distinct, i.e., some collapsing clouds may appear to be in turbulent equilibrium.

IV. PROXIMITY TO YOUNG STARS

The dense cloud cores described in this paper can be best examined for proximity to young stars in the Taurus-Auriga complex because: (1) this region was surveyed heavily and gave many detections in the NH_3 line; (2) it is well studied optically, with large-scale coverage in objective prism surveys for emission-line stars down to ~ 14 mag (Herbig 1962) and with ~ 100 young stars believed to be associated with the gas (Jones and Herbig 1979; Cohen and Kuhi 1979); and (3) the observations of Cohen and Kuhi permit estimates of stellar ages and star formation rates.

Figure 4 shows the distribution of emission-line stars in Taurus-Auriga as small filled circles. Stars were included if they appear either in the list of probable members measured for proper motion by Jones and Herbig (1979; 79 stars) or in the list of emission-line stars observed in the same region by Cohen and Kuhi (1979; 32 additional stars). The distribution of stars is slightly different from that in Figure 2 of Jones and Herbig because the added stars from Cohen and Kuhi enhance the appearance of clustering. The stars can be divided into seven groups where the star surface density exceeds five stars per square degree. This division is consistent with that of Jones and Herbig, who distinguished three of these groups: I (labeled L1495 in Figure 4), IIa (TMC-2), and III (L1551). Jones and Herbig considered the stars near TMC-1, B217, and L1536 as members of a more diffuse group (group II). However, when the 32 additional stars from Cohen and Kuhi are included, group II appears to break into three parts, and the five stars near L1517 appear to form a

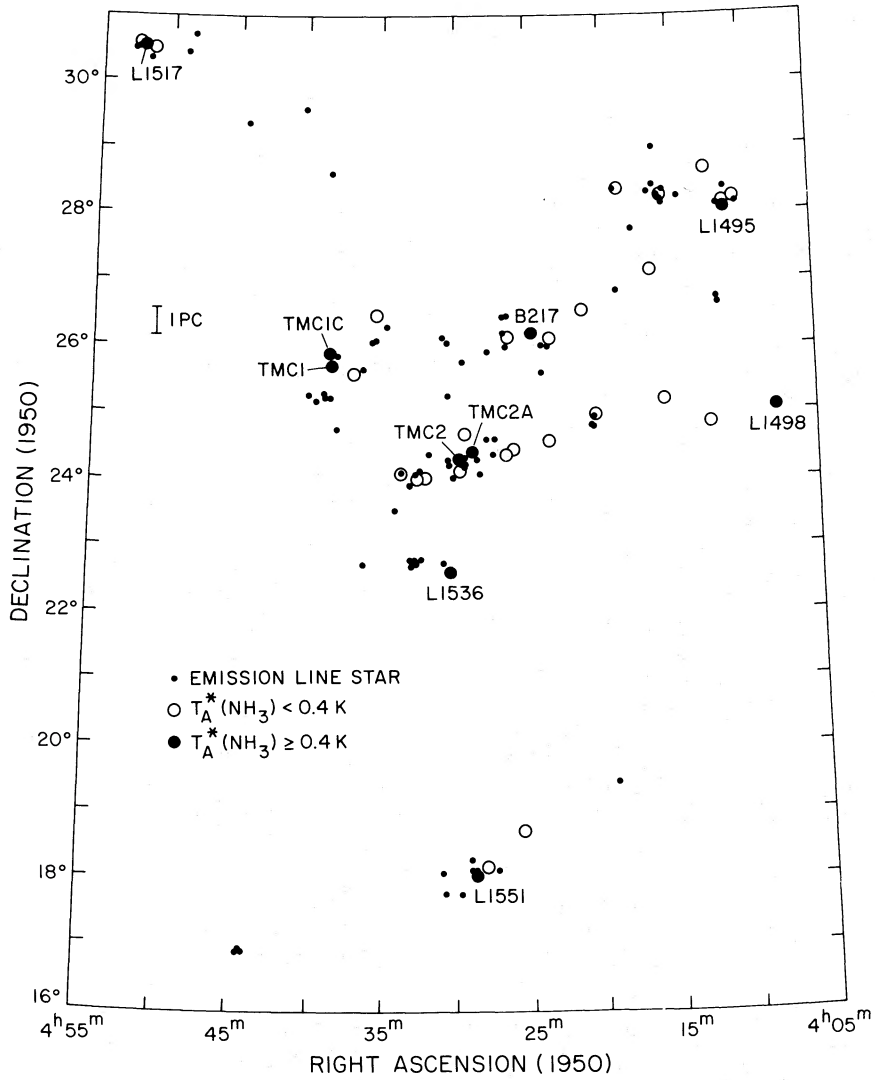

FIG. 4.—Comparison of positions of emission-line stars in Taurus-Auriga (*small filled circles*) with positions where dense cores were sought and found (*large filled circles*) or sought and not found (*large open circles*). Dense cores were found more frequently in groups of emission-line stars (9 out of 20) than away from groups of emission-line stars (1 out of 8).

distinct group. The resulting seven groups are then near L1495, B217, L1551, TMC-2, L1536, TMC-1, and L1517.

Superposed on this picture are positions surveyed for NH_3 emission on the basis of high visual obscuration, either in this survey or in that of Myers, Ho, and Benson (1979). Positions where the line intensity was weak or absent [$T_A^*(NH_3) < 0.4$ K] are shown as large open circles; positions of strong emission [$T_A^*(NH_3) \geq 0.4$ K] are shown as large filled circles. All of the regions of strong emission ("dense cores") were mapped and are included among the sources summarized in Table 1.

Figure 4 shows a close association between dense cores and groups of emission-line stars. At least one dense core is associated with each group. There also appears to be a preferential association between dense cores and star groups, which is more specific than the association between opaque regions and star groups. We attempted to examine this quantitatively by drawing seven ellipses, each of which just enclosed all the stars in a group. Then the fraction of surveyed positions (*open or filled large circles*) which are dense cores (*filled large circles*) is $9/20 = 0.45$ inside star groups and $1/8 = 0.13$ outside groups. If the criterion for association is relaxed by doubling each linear dimension of each ellipse, then the three central groups (containing TMC-1, TMC-2, and B217) merge together, and the dense core fraction is $9/24 = 0.38$ inside groups and $1/4 = 0.25$ outside groups. If each ellipse dimension is tripled, five groups merge together, and the dense core fraction is $9/25 = 0.36$ inside groups and $1/3 = 0.33$, negligibly different, outside groups. This comparison suggests that the dense core fraction inside groups may or may not be significantly greater than that outside groups, depending on the criterion for association. However, if, as seems reasonable, one chooses boundaries which make the three central groups in Figure 4 distinct, then the dense cores appear to be preferentially associated with the star groups. This suggests that the dense cores are probably closely related to the star formation process.

The actual number of dense cores in Taurus-Auriga is probably greater than we have observed. The NH_3 survey is far from complete, since only $\sim 10^{-3}$ of the surface area containing groups of emission-line stars was actually surveyed. If the yet undiscovered dense cores are similar to those in Table 1 and have normal gas-to-dust ratios, then they typically have $A_v \sim 10$ mag and should appear as localized regions of high visible obscuration. The number of regions with this appearance within the boundaries of Figure 4 is uncertain because of masking by extended obscuration and fluctuations in illuminating starlight, but we estimate that there are 87 such regions, of which we have surveyed 39. This suggests that the number of dense cores in Taurus-Auriga which resemble those we have found is of the order of 25.

The association evident in Figure 4 between dense cores and groups of emission-line stars is consistent with the well-known association of emission-line stars and visible obscuration but has several additional implications of importance to star formation. First, the association of groups of emission-line stars and dense cores appears more detailed than the association of emission-line stars and obscuration, as described above. Since strong NH_3 emission requires density $\gtrsim 10^4$ cm^{-3}, it may be that the high-extinction regions away from groups of emission-line stars have more extended, low-density gas distributions with relatively less internal condensation, while the high-extinction regions near groups of emission-line stars have more density contrast and "clumping." Second, the typical dense core associated with a group of emission-line stars has the mass needed to form one or two low-mass stars and has the stability characteristics, described in § III, expected for a region which has recently begun, or will soon begin, to collapse.

Third, the number of known or expected cores in Taurus-Auriga (10–25) agrees in order of magnitude with the numbers of stars (25–50) expected to form in the next free-fall time. The optical and infrared observations of Cohen and Kuhi (1979) permit estimates, uncertain by a factor of $\gtrsim 2$, of the time elapsed since formation of the stellar core. Cohen and Kuhi found that the distribution of ages in Taurus-Auriga implies an onset of star formation at $\sim 6 \times 10^6$ years ago, followed by continuous exponential growth in the number of stars, with a doubling time of $\sim 6 \times 10^5$ yr. For a typical dense core density of 3×10^4 cm^{-3}, the free-fall time is 2×10^5 yr. According to the birthrate estimate of Cohen and Kuhi, in this period the population of young stars in Taurus-Auriga will increase by a factor of 1.26. The number of known emission-line stars in Taurus is ~ 100, but a significant number of additional, optically invisible stars could be embedded in these clouds. Jones and Herbig (1979) considered this question by modeling the visible obscuration in Taurus-Auriga and by using 48 emission-Hα stars for which estimates of A_v were available from Cohen and Kuhi (1979). Their model predicts 176 emission-Hα stars brighter than $M_{pg} = 9.5$ mag (corresponding to the Cohen and Kuhi survey limit). The number of additional fainter stars is uncertain. We estimate a probable upper limit to the number of additional stars by assuming that the luminosity function, Ψ_1 (M_{pg}), of Jones and Herbig is flat from $M_{pg} = 9.5$ mag to $M_{pg} = 12$ mag, and zero beyond 12 mag, where very few T Tauri stars are known (Herbig 1962); then there are less than 36 additional stars, and the total is less than 212. Similar modeling by Jones and Herbig of available 2 μm data in the Taurus clouds indicates that the surface density of associated infrared sources, averaged over the entire area of obscuration, as 0.38 pc^{-2}. Estimating the area of obscuration is 390 pc^2, the expected number of 2 μm sources in the Taugus-Auriga complex is 148. Jones and Herbig concluded that there is no evidence for a large concentration of faint infrared sources toward cloud centers in Taurus-Auriga. Based on these estimates, we assume that the number of young stars in Taurus lies in the range 100–200, so that some 25–50 new stars should form in the next 2×10^5 yr. This number of stars is

in reasonable agreement with the known (10) or expected (25) number of dense cores, particularly since some cores may be expected to form binary stars. The agreement is much better than that which results from comparing the rate of star formation in the galaxy, 1–4 stars per year, with the total mass in molecular clouds divided by the typical free-fall time, greater than 30 $M_\odot$ yr^{-1} (Zuckerman and Palmer 1974). These comparisons can be consistent if only a small fraction of the total cloud mass converts completely to stars on the free-fall time scales.

The exponential growth law of Cohen and Kuhi (1979) is based on the entire Taurus-Auriga complex, and it is possible that some regions in the complex have stopped producing stars, while others are forming stars much more rapidly than the average. If so, one might expect the distribution of dense cores to reflect these differences if they are indeed future stars. We have examined the stellar ages within each of the seven groups in Figure 4. Although there are differences in mean age, these are slight. Each group has at least two stars younger than 6×10^5 yr, and each group except that near L1536 has at least one star younger than 3×10^5 yr. Therefore, there is no clear indication that any of the emission-line star groups in Figure 4 has stopped producing stars; and no reason based on stellar ages to expect a significant difference in dense core population from group to group.

In summary, there is a detailed association of dense cores and groups of emission-line stars in Taurus-Auriga, evident in Figure 4; and there is reasonable agreement between the number of dense cores and the number of stars expected to form in the next free-fall time. These results suggest that many, if not all, of the 10 known dense cores in Taurus-Auriga are likely to form low-mass stars within the next few free-fall times.

V. DISCUSSION

The line shape and stability analyses in § III, indicate that most of the dense cores described here are consistent with early collapse or near-critical equilibrium. The comparison of core with star group positions and the comparison of core collapse with star formation rates in § IV indicate that many of the dense cores will form stars in the next $\sim 10^6$ yr. These results appear to present a consistent picture, in which the dense cores are now forming, or will soon form, low-mass stars. The interpretation of molecular line observations in terms of collapse to form stars is well known. However, the use of the Jeans length or similar analysis, by itself, to reach this conclusion is unlikely to be convincing because the same analysis which says that a cloud is unstable when supported only by thermal motions often says that it is stable when supported by the Doppler motions in its line width (Larson 1981). Figure 3 shows that this ambiguity is present in the regions studied here. The new and more decisive aspect of this study comes from the comparison with stellar data. The association of dense cores and groups of emission-line stars in Figure 4 and the agreement between dense core collapse rates and star formation rates described in § IV place the conclusion of ongoing or incipient collapse on a firmer footing than was possible before. Still, the case is circumstantial, and it would be desirable to have a direct observational signature of a collapsing region, such as the wings shown in Figure 1*b*. One might speculate that, if such wings were not found, the collapse process might be much shorter or much longer than the free-fall time. If it were much shorter, the likelihood of finding a region during this period would be reduced; if it were much longer, the expected wings would be much smaller than in Figure 1*b* and difficult to detect.

For the present, we examine ways in which the conclusions presented here might be in error. It is conceivable that the number of regions with $n \sim 10^4$ cm^{-3} in Taurus-Auriga is actually much greater than the ~ 25 estimated from the statistics of detecting NH_3 emission from visually obscured regions. This could arise if the gas-to-dust ratio varied significantly from dense core to dense core, so that many dense regions would appear nearly transparent and would escape being counted and surveyed. This question can be tested by full-coverage surveys, possibly in the NH_3 line, of selected areas containing high and low concentrations of emission-line stars. Then the conclusions would not be biased by selection based on visual obscuration. However, there does not appear to be evidence now available which would support significant variations in the gas-to-dust ratio in dense clouds.

It is possible that the dense cores are not as highly correlated with the groups of emission-line stars as the present data suggest. The detection rate of dense cores away from emission-line star groups (1/8) would be comparable to that in or near emission-line star groups (9/20) if only two or three of the negative surveyed positions proved positive. Further observations are needed to reduce the uncertainty in the control group.

It is also possible that the dense cores are simply associated with star formation regions but are not future stars; rather, they might be stable condensations which can survive for relatively long periods in quiescent dark clouds, where strong perturbations due to shocks and ionization fronts are largely absent. In this picture, the coincidence between the expected star formation rate and the expected dense core collapse rate is fortuitous. However, it is then necessary to explain the origin of the 25–50 stars expected to form in Taurus-Auriga in the next few times 10^5 yr. If the gas which will form these stars is not now in prestellar condensations, it will soon have to be compressed by a process that is rapid compared with free-fall, which seems unlikely. If the gas which will form these stars is now in prestellar condensations which are distinctly different from the dense cores discussed here, such condensations probably have to be much denser and smaller than the dense cores (e.g., $n \gtrsim 10^6$ cm^{-3}, $R \lesssim 0.03$ pc). Then such "superdense" cores could escape detection with present-day observations. It does not appear possible to rule out such objects on observational or theoretical

grounds, but there is no evidence for their existence at present.

If the dense cores described here are future stars, it is of interest to know how many are in late collapse, with embedded cores; how many are in early collapse, without stellar cores; and how many have not yet begun to collapse. Further infrared and spectral line observations are needed to attempt to answer these questions. At present, four of the dense cores in Table 1 have some evidence of associated stellar cores within their half-maximum map contours: L1551, L43, TMC-2, and B335. The strongest case is L1551, which has an embedded infrared source (Strom, Strom, and Vrba 1976), bipolar molecular outflow (Snell, Loren, and Plambeck 1980), and radio continuum emission (Cohen, Bieging, and Schwartz 1982). L43 has an optically visible red star, RNO 91 in the catalog of Cohen (1980), whose reflection nebulosity indicates association with the dark cloud (Herbst and Warner 1981). TMC-2 also known as L1529, has localized CO wings ~ 30 km s^{-1} wide, but no known infrared source (Lichten 1982). B335 has CO wings suggestive of outflow (Frerking and Langer 1982) and may have a far-infrared source (Davidson *et al.* 1982). It is possible that some, but probably not all, of these apparent associations are cases of coincidence along the line of sight. Therefore, probably $\gtrsim 15\%$ of the dense cores in Table 1 have embedded stellar cores. We note that, if the broad outflow wings in L1551 and TMC-2 are a common and long-lived facet of early stellar evolution, their presence may hamper identification of the narrower wings expected for purely collapsing regions.

If many of the dense cores described here can be regarded as future stars which have not yet formed stellar cores, there will be many new opportunities to study this extremely early stage of stellar evolution. It will be possible to make systematic surveys of molecular clouds for such regions, to estimate the number and distribution of future low-mass stars. These can be compared with similar studies of optically invisible, embedded infrared sources and of optically visible emission-line stars. It will be of interest to survey for dense cores in star-forming regions which are less vigorously producing young stars, such as NGC 7000 (Cohen and Kuhi 1979), and in regions which are primarily producing more massive stars.

It should be noted that the NH_3 observations described here represent one of several molecular line probes which are useful in identifying small dense regions. Others include the 2 cm and 2 mm lines of H_2CO (Evans and Kutner 1976), the higher rotational lines of HC_3N (Avery 1980), and the 7 mm and 3 mm lines of CS (Linke and Goldsmith 1980). All of these lines have brightness temperatures in dark clouds $\lesssim 1$ K, so that full-coverage surveys of molecular clouds with telescope beamwidth $\lesssim 1'$ are extremely time-consuming. It appears necessary to precede such observations with a more rapid "finding" survey such as the visual survey of Palomar Sky Survey prints for obscuration that was done in this work. However, as telescope and receiver technology improve, this will become less of a limitation.

VI. SUMMARY

The main points presented in this paper are:

1. A survey of ~ 100 visually opaque regions in relatively nearby dark clouds has been made in the 1.3 cm $(J, K) = (1, 1)$ line of NH_3, with (1, 1) line mapping and (2, 2) line observations in selected regions. There are 27 "dense cores" which have been mapped and which have reliable distance estimates. The mean source properties are: size, 0.1 pc; density, 3×10^4 cm^{-3}; mass, 4 $M_\odot$; kinetic temperature, 11 K; and FWHM velocity width, 0.3 km s^{-1}.

2. For six sources with sufficiently strong and narrow lines, the intrinsic line shape has been estimated from the spectra and compared to cloud motion models involving purely thermal motions, thermal and microturbulent motions, thermal motions and uniform rotation, and thermal and collapse motions. The intrinsic line shapes are essentially Gaussian and are best fitted by either thermal and subsonic microturbulent motions, or thermal and collapsing motions, where the collapse is early enough ($< 10^5$ yr) that a stellar core has not yet formed.

3. The source densities, sizes, and temperatures (kinetic and Doppler) have been compared with equilibrium and stability requirements of a spherical, isothermal, nonuniform cloud bounded by a medium of constant pressure. This indicates that if the observed clouds are supported only by thermal motions, they are either collapsing or in unstable equilibrium. If they are supported by their Doppler motions, they are either collapsing or in near-critical equilibrium. In this latter case, the data points lie close to the critical line.

4. The ~ 100 known young emission-line stars in Taurus-Auriga can be divided into seven spatial groups which have more than five stars per square degree. The dense cores detected in this survey appear to be associated with these groups, although they were selected to be surveyed on the basis of obscuration rather than proximity to stars. Every group has at least one dense core; the fraction of visually obscured regions having dense cores is greater in the groups of emission-line stars (9/20) than outside the groups (1/8).

5. The studies of Cohen and Kuhi (1979) and Jones and Herbig (1979) indicate that the Taurus-Auriga complex is likely to form 25–50 emission-line stars in the next 2×10^5 yr, which is one free-fall time for the typical dense core. This number of stars agrees well with the estimated number of dense cores in Taurus-Auriga, 25, based on the 10 which we found and the fraction of obscured regions which we searched.

6. The cloud motion analysis, the comparison of emission-line star with dense core positions, and the comparison of the expected number of new stars with the number of dense cores in Taurus-Auriga appear to have the common interpretation that most, if not all, of the dense cores described here will form low-mass stars in the next few free-fall times ($\sim 10^6$ yr).

We wish to thank the administrative and technical staffs of Haystack Observatory and the National Radio

Astronomy Observatory for their support during the observations. P. J. B. thanks Zonta International for an Amelia Earhart Fellowship. P. C. M. thanks the National Academy of Sciences–National Research Council for a Research Associateship and the NASA Goddard Institute for Space Studies for their hospitality during the early part of this work; and the Harvard-Smithsonian Center for Astrophysics for their hospitality during the completion of this work. This research was partly supported by NSF grant AST 81-21416.

REFERENCES

Ambartsumian, V. A. 1947, *Stellar Evolution and Astrophysics* (Yerevan: Acad. Sci. Armenian S.S.R.).
Avery, L. W. 1980, in *Interstellar Molecules*, ed. B. Andrew (Boston: Reidel), p. 47.
Ball, J. A. 1975, in *Methods in Computational Physics*, Vol. **14**, *Radio Astronomy*, ed. B. Adler, S. Fernbach, and M. Rotenberg (New York: Academic), p. 214.
Benson, P. J., and Myers, P. C. 1980, *Ap. J. (Letters)*, **242**, L87 (BM).
Bok, B. J., and McCarthy, C. C. 1974, *A.J.*, **79**, 42.
Bonnor, W. B. 1956, *M.N.R.A.S.*, **116**, 351.
Buxton, R. B. 1981, Ph.D. thesis, Massachusetts Institute of Technology.
Cohen, M. 1980, *A.J.*, **85**, 29.
Cohen, M., Bieging, J. H., and Schwartz, P. R. 1982, *Ap. J.*, **253**, 707.
Cohen, M., and Kuhi, L. V. 1979, *Ap. J. Suppl.*, **41**, 743.
Davidson, J. A., Harper, D. A., Hildebrand, R. H., Keene, J., and Low, F. J. 1982, paper presented at American Astronomical Society Meeting, Troy, New York.
Ebert, R. 1955, *Zs. Ap.*, **37**, 217.
Elias, J. H. 1978*a*, *Ap. J.*, **224**, 857.
———. 1978*b*, *Ap. J.*, **224**, 453.
Elmegreen, D. M., and Elmegreen, B. G. 1978, *Ap. J.*, **220**, 510.
Evans, N. J., and Kutner, M. L. 1976, *Ap. J. (Letters)*, **204**, L131.
Field, G. B. 1978, in *Protostars and Planets*, ed. T. Gehrels (Tucson: University of Arizona Press), p. 243.
Frerking, M. A., and Langer, W. D. 1982, *Ap. J.*, **256**, 523.
Goldreich, P., and Kwan, J. 1974, *Ap. J.*, **189**, 441.
Green, S. 1980, *J. Chem. Phys.*, **73**, 2740.
Herbig, G. H. 1962, *Adv. Astr. Ap.*, **1**, 47.
Herbst, W., and Warner, J. W. 1981, *A.J.*, **86**, 885.
Jones, B. F., and Herbig, G. H. 1979, *A.J.*, **84**, 1872.
Joy, A. H. 1945, *Ap. J.*, **102**, 168.
———. 1949, *Ap. J.*, **110**, 424.
Kukolich, S. G. 1967, *Phys. Rev.*, **156**, 83.
Langer, W. D., Goldsmith, P. F., Carlson, E. R., and Wilson, R. W. 1980, *Ap. J. (Letters)*, **235**, L39.
Larson, R. B. 1972, *M.N.R.A.S.*, **157**, 121.
———. 1979, *M.N.R.A.S.*, **186**, 479.
———. 1981, *M.N.R.A.S.*, **194**, 809.
Lichten, S. M. 1982, *Ap. J. (Letters)*, **255**, L119.
Linke, R. A., and Goldsmith, P. A. 1980, *Ap. J.*, **235**, 437.
Little, L. T., MacDonald, G. H., Riley, P. W., and Matheson, D. N. 1979, *M.N.R.A.S.*, **189**, 539.
Martin, R. N., and Barrett, A. H. 1978, *Ap. J. Suppl.*, **36**, 1.
Mattila, K. 1979, *Astr. Ap.*, **78**, 253.
Myers, P. C., Ho, P. T. P., and Benson, P. J. 1979, *Ap. J. (Letters)*, **234**, L144.
Myers, P. C., Linke, R. A., and Benson, P. J. 1963, *Ap. J.*, **264**, 517. (Paper I).
Scoville, N. Z., and Solomon, P. M. 1974, *Ap. J. (Letters)*, **187**, L67.
Shu, F. 1977, *Ap. J.*, **214**, 488.
Snell, R. L. 1981, *Ap. J. (Suppl.)*, **45**, 121.
Snell, R. L., Loren, R. B., and Plambeck, R. L. 1980, *Ap. J. (Letters)*, **239**, L17.
Spitzer, L. 1968, in *Stars and Stellar Systems*, Vol. **7**, *Nebulae and Interstellar Matter*, ed. B. M. Middlehurst and L. H. Aller (Chicago: University of Chicago Press), p. 1.
———. 1978, *Physical Processes in the Interstellar Medium* (New York: Wiley).
Strom, K. M., Strom, S. E., and Vrba, F. J. 1976, *A.J.*, **81**, 308.
Ungerechts, H., Walmsley, C. M., and Winneswisser, G. 1980, *Astr. Ap.*, **88**, 259.
———. 1982, *Astr. Ap.*, **111**, 339.
Wilson, W. J., Schwartz, P. R., Epstein, E. E., Johnson, W. A., Etcheverry, R. D., Mori, T. T., Berry, G. G., and Dyson, H. B. 1974, *Ap. J.*, **191**, 357.
Zuckerman, B., Buhl, D., Palmer, P., and Snyder, L. E. 1970, *Ap. J.*, **160**, 485.
Zuckerman, B., and Evans, N. J. 1974, *Ap. J. (Letters)*, **192**, L149.
Zuckerman, B., and Palmer, P. 1974, *Ann. Rev. Astr. Ap.*, **12**, 279.

PRISCILLA J. BENSON: Room 26–348, Massachusetts Institute of Technology, Cambridge, MA 02139

PHILIP C. MYERS: Room D312, Center for Astrophysics, 60 Garden Street, Cambridge, MA 02138